

Superinfecting mycobacteria home to established tuberculous granulomas

Christine L Cosma¹, Olivier Humbert¹ & Lalita Ramakrishnan^{1,2,3}

A central paradox of tuberculosis immunity is that reinfection and bacterial persistence occur despite vigorous host immune responses concentrated in granulomas, which are organized structures that form in response to infection. Prevailing models attribute reinfection and persistence to bacterial avoidance of host immunity via establishment of infection outside primary granulomas. Alternatively, persistence is attributed to a gradual bacterial adaptation to evolving host immune responses. We show here that superinfecting *Mycobacterium marinum* traffic rapidly into preexisting granulomas, including their caseous (necrotic) centers, through specific mycobacterium-directed and host cell-mediated processes, yet adapt quickly to persist long term therein. These findings demonstrate a failure of established granulomas, concentrated foci of activated macrophages and antigen-specific immune effector cells, to eradicate newly deposited mycobacteria not previously exposed to host responses.

The enormous global burden of tuberculosis is exacerbated by bacterial persistence and reinfection. Infection of humans with *Mycobacterium tuberculosis*, one of the causative agents of tuberculosis, is thought to often result in a state of clinical latency in which the bacteria may persist undetected for decades before leading to active disease^{1–3}. As for reinfection, early epidemiological studies suggested that natural *M. tuberculosis* infection afforded some protection against subsequent infection⁴. However, molecular fingerprinting analyses have demonstrated that this protection is far from complete: reinfection accounts for a substantial proportion of active tuberculosis cases in high-prevalence areas^{5,6}. Furthermore, the live attenuated *Mycobacterium bovis* vaccine strain, bacille Calmette-Guerin, has been mostly ineffective in protecting against adult tuberculosis in large scale clinical trials⁷. Similarly, various attenuated strains of *M. tuberculosis* and genetically engineered derivatives of bacille Calmette-Guerin have not improved protection substantially in animal models of infection^{7–9}.

Reinfection and persistence occur at an appreciable frequency despite the robust adaptive immune response that usually results from primary infection^{2,3,7}. Immunity to tuberculosis is concentrated in complex immune structures called granulomas that comprise differentiated macrophages, lymphocytes and other immune cells, as well as extracellular matrix components^{2,3,7}. Within granulomas, bacteria are found both in macrophages and in central areas of necrosis called caseum that develop in mature lesions^{10,11}. The various elements of the granuloma are thought to act in concert to thwart and contain the bacteria. The presence of a functional adaptive immune response is essential for granuloma maintenance and

for curtailment of infection^{2,7}. Indeed, loss of such immunity in humans, as occurs, for example, in human immunodeficiency virus infection, is associated with a lack of granuloma integrity and more disseminated and lethal forms of tuberculosis^{12,13}. Similarly, mice engineered to have specific deficiencies in cell-mediated immunity have poor granulomas and succumb to disseminated infection². A fundamental puzzle, then, is why and how bacterial persistence and reinfection occur in the face of adaptive immune responses that seem to be protective to a large extent. As is the case with many persistent infections, the requirements for a sterilizing immunity to tuberculosis remain elusive.

Various models have been proposed to explain the ability of mycobacteria to defy host immunity in the context of reinfection and persistence. With respect to persistence, some models propose that bacteria are sequestered in the caseum, where they may reside indefinitely, protected from killing by host immune cells^{10,11,14}. Other models hypothesize that primary granulomas provide effective, localized antimycobacterial immunity, but that some bacteria escape these loci¹⁵ and persist in new sites proposed to be anatomically or immunologically vulnerable^{16,17}. The latter models have been further used to explain reinfection: newly infecting bacteria avoid previously established immune foci and form new foci of infection in these vulnerable regions^{16–18}. Notably, these critical steps in tuberculosis pathogenesis are based on human epidemiological studies and indirect evidence from animal models.

To directly examine the dynamics of mycobacterium reinfection *in vivo*, we tracked the path of a superinfecting *Mycobacterium marinum* strain in the context of previously established granulomatous infections

Departments of ¹Microbiology, ²Immunology and ³Medicine, University of Washington School of Medicine, Box 357242, Seattle, Washington 98195, USA. Correspondence should be addressed to L.R. (lalitar@u.washington.edu).

Published online 27 June 2004; doi:10.1038/ni1091

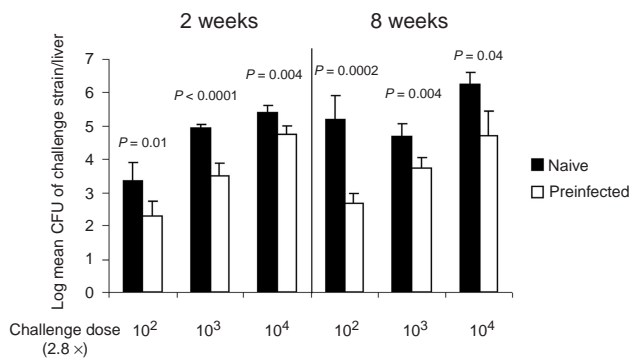


Figure 1 Preexisting infection confers immunity to a low-dose secondary infection. Uninfected frogs (Naive), and frogs previously infected for 6 weeks with 3.3×10^6 CFU wild-type *M. marinum* (Preinfected), were infected with 2.8×10^2 to 2.8×10^4 CFU (horizontal axis) of an isogenic strain carrying a plasmid for kanamycin resistance. Kanamycin-resistant bacteria were counted in liver and spleen 2 and 8 weeks later. Data represent means (with s.d.) of log CFU/liver of three to five frogs. *P* values are for differences between means of preinfected and naive animals (Student's unpaired *t*-test). At the 2-week time point, one preinfected frog inoculated with 2.8×10^2 superinfecting bacteria and one preinfected frog inoculated with 2.8×10^3 superinfecting bacteria did not have any detectable organisms and these were not included in the calculation of the mean. We obtained similar results with the spleen (data not shown).

in leopard frogs (*Rana pipiens*) and zebrafish (*Danio rerio*). *M. marinum*, the mycobacterium most closely related to organisms of the *M. tuberculosis* complex (http://www.sanger.ac.uk/Projects/M_marinum/), causes systemic chronic tuberculosis in ectotherms and peripheral granulomatous disease in humans³. *M. marinum* infection in these natural hosts serves as an excellent model for tracking mycobacteria *in vivo*, because like *M. tuberculosis* infection in humans, *M. marinum* infection of frogs produces discrete, highly organized paucibacillary granulomas that contain the infecting bacteria indefinitely^{19,20}. In addition, *M. marinum* granulomas in zebrafish develop caseous centers similar to those caused by infection of humans by *M. tuberculosis*, affording the opportunity to study this ill-understood entity^{3,20,21}. Like *M. tuberculosis* granulomas in mammals, *M. marinum* granulomas in both frogs and fish contain lymphocytes that are required for granuloma maintenance^{19,20}. *M. marinum* and *M. tuberculosis* share virulence determinants³ and, likewise, fish and mammals have similar innate and adaptive immune responses²². Consequently, *M. marinum* studies in these natural hosts have yielded important insights about the bacterial and host factors involved in granuloma formation^{20,23–26}. Indeed *M. marinum* is being increasingly used as a surrogate model to study host-pathogen interactions in tuberculosis^{3,20,21,27,28} akin to the widespread use of *Salmonella enterica* serovar Typhimurium in the mouse to understand human typhoid fever, caused by *Salmonella enterica* serovar Typhi²⁹.

Here we report our in-depth examination of the trafficking and fate of reinfecting mycobacteria in the context of preexisting tuberculosis. Using frog and zebrafish models of tuberculosis, we show that superinfecting mycobacteria were rapidly and specifically transported into pre-established granulomas by host mononuclear cells. These bacteria further made their way into the caseum, a space previously thought to be mostly secluded. This host-directed

trafficking did not affect the long-term survival of the reinfecting bacteria. These results suggest that the ability of mycobacterium to persist in and to reinfect immune hosts is due to a fundamental failure of host immunity to eradicate the infection rather than to mechanisms developed by these pathogens to physically avoid foci of host immunity.

RESULTS

Protection against *M. marinum* superinfection in preinfected frogs

Animal models of *M. tuberculosis* infection mirror the lack of clinical protection in humans. Mice and guinea pigs with past or ongoing infection of *M. tuberculosis*, or those that have been vaccinated using a variety of protocols, have a lower tissue burden of a reinfecting or superinfecting strain than do naive animals^{30,31}. Nevertheless, persistent infection with the second strain is achieved, even at very low challenge doses^{30,31}. Therefore, we first determined whether frogs chronically infected with *M. marinum* also have partial immunity to superinfection. We infected frogs with wild-type *M. marinum* through intraperitoneal injection and superinfected the frogs 6 weeks later with tenfold dilutions of a kanamycin-resistant strain. We determined the burden of superinfecting bacteria in liver and spleen at 2 and 8 weeks after superinfection. At both times, the burden of the superinfecting strain was 1–2 logs less in preinfected frogs than in naive frogs. At 2 weeks, 13 of 15 frogs had detectable numbers of the challenge strain (Fig. 1), and by 8 weeks all frogs were superinfected, even when as few as 2.8×10^2 superinfecting bacteria were injected (Fig. 1). These findings parallel those in mammalian models of *M. tuberculosis* infection^{30,31}, verifying that immunity to mycobacterial infections is functionally similar in frogs and mammals.

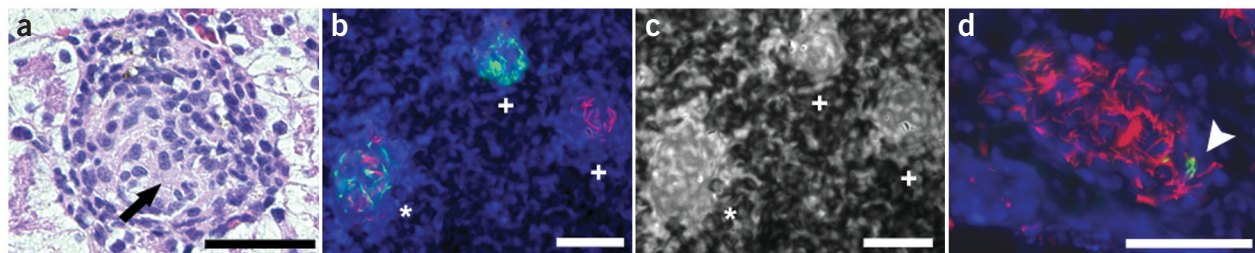


Figure 2 Long-term superinfection of frogs results in comingling of primary and secondary infecting strains. Frogs were infected with 3×10^6 CFU red fluorescent *M. marinum* for 8 weeks and then were superinfected with 9×10^5 CFU green fluorescent *M. marinum* for an additional 10 weeks. (a) Typical liver granuloma at 8 weeks after infection, stained with hematoxylin and eosin; arrow indicates epithelioid macrophages. (b–d) Combined fluorescence images show red and green fluorescent *M. marinum* as well as DAPI-stained tissue nuclei in blue. (b) Spleen tissue after an 8-week preinfection and a 10-week superinfection. (c) Monochromatic image of DAPI fluorescence from b, emphasizing the dense concentration of host immune cells in the granuloma. In b,c: +, single-strain granulomas; *, mixed granulomas. (d) Mixed granuloma in lung; arrowhead indicates green bacteria. Scale bars, 50 μ m.

Mycobacteria transport to established granulomas via host cells

We next used microscopic analyses of tissues to determine the localization of superinfecting bacteria with respect to previously established granulomas. We first infected frogs with red fluorescent *M. marinum* for 8 weeks to establish chronic granulomatous infection (Fig. 2a) and then superinfected the frogs with green fluorescent bacteria. At 10 and 20 weeks after superinfection, we collected tissues and examined frozen sections 10 μm in thickness from liver, spleen and lung. In all tissues, many granulomas contained both red and green fluorescent bacteria, suggesting that the superinfecting strain penetrated readily and persisted in previously established granulomas (Figs. 2b–d and 3 and data not shown). Longer preinfection periods did not alter the ability of superinfecting organisms to infiltrate preexisting lesions (data not shown). The superinfecting strain also established its own granulomas (Figs. 2b and 3b). To confirm that the mixed granulomas found several weeks after superinfection represented trafficking of superinfecting bacteria into established granulomas rather than remodeling of adjacent granulomas first established separately by the two strains, we superinfected frogs as described above and examined the localization of the superinfecting strain 3 d after superinfection. We counted individual green fluorescent bacteria in liver sections; on average, 29% were inside pre-existing granulomas, demonstrating rapid trafficking of superinfecting bacteria (Figs. 4 and 5 and Supplementary Table 1 online).

Uninfected macrophages are reported to continuously enter the cellular layers of bacille Calmette-Guérin-induced granulomas in

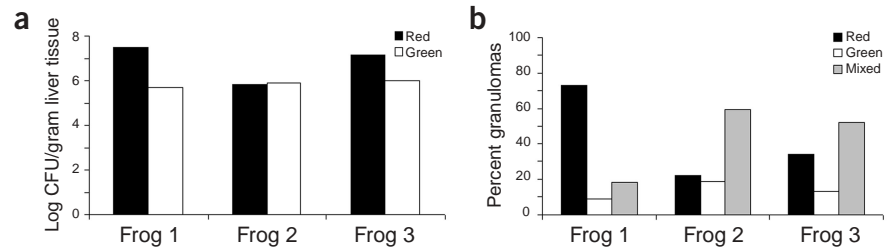


Figure 3 Distribution of preinfecting and superinfecting *M. marinum* strains in frog tissues after long-term infection. Frogs were infected as described in Figure 2. (a) Relative proportions of green and red fluorescent CFU, determined by examination of colonies on plates; those expressing red fluorescence appear red on solid medium, whereas those expressing green fluorescence do not. (b) Percent red, green or mixed granulomas, determined by counting of a total of 90–271 granulomas in one to three sections of liver tissue.

rabbits¹⁴. Also, during primary infection, host mononuclear cells transport mycobacteria from the initial infection site to deeper tissues^{24,32–34}. Therefore, we next sought to determine whether the superinfecting mycobacteria were gaining passage into established granulomas within host cells. To examine this trafficking, we used a red fluorescent strain of *M. marinum* that expresses green fluorescent protein (GFP) from a macrophage-activated promoter induced by entry into host cells²³. With this strain, all bacteria are red fluorescent, but only those located intracellularly are green fluorescent^{23,26}. We used this doubly marked strain to superinfect frogs previously infected with cyan fluorescent *M. marinum*. At 3 d after superinfection, dually red and green fluorescent bacteria were within (Fig. 4b) and outside (Fig. 4c) preexisting granulomas, indicating that they were intracellular. Almost all (98%) of the red fluorescent bacteria located outside of lesions were also green fluorescent (Fig. 4c and

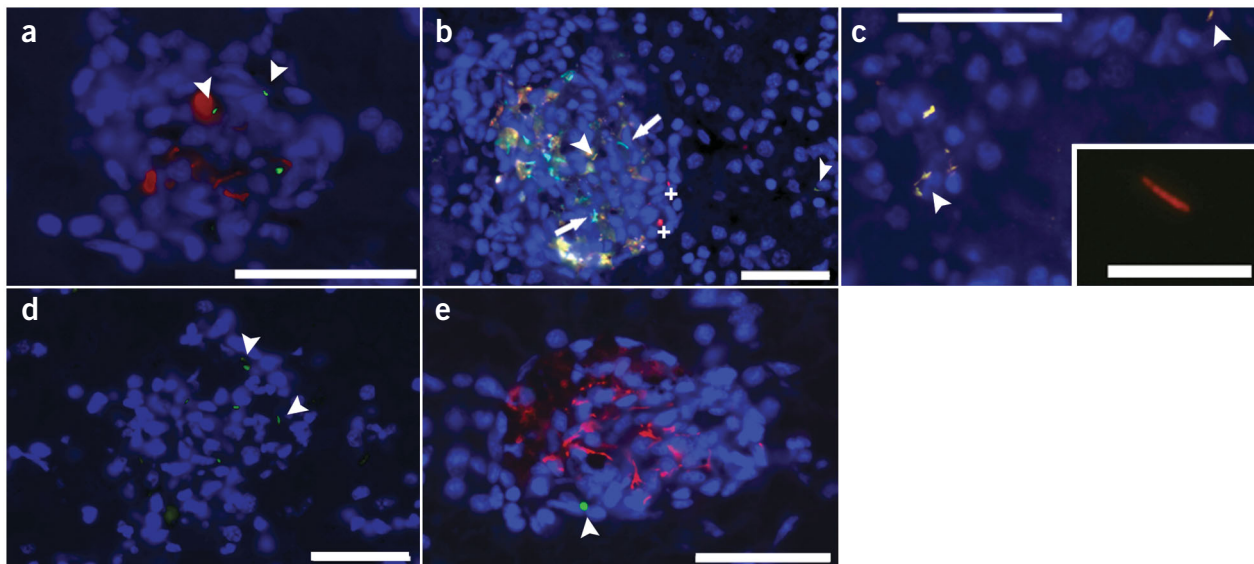
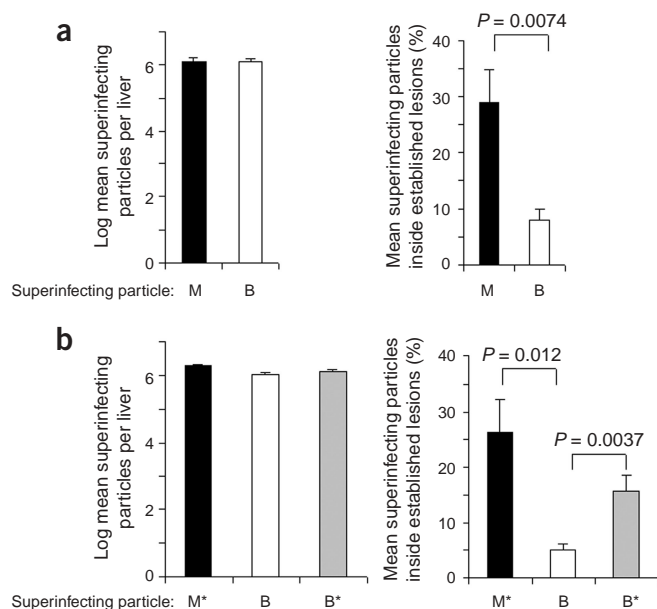


Figure 4 Superinfecting bacteria and beads traffic into pre-established granulomas. Frogs were infected and superinfected, and tissues were collected 3 d after superinfection, then combined fluorescence images of liver granulomas were obtained. (a) Frogs were infected with 2.3×10^6 CFU red fluorescent *M. marinum* and were then superinfected 7 weeks later with 3.8×10^6 CFU green fluorescent *M. marinum*. (b,c) A frog was infected with 4.5×10^6 CFU cyan fluorescent bacteria for 6.5 weeks and then was superinfected with 4.5×10^7 CFU double-labeled bacteria, which appear yellow here because of overlap of green and red fluorescence. Arrow, cyan bacteria; +, tissue autofluorescence. Inset in c, doubly marked strain grown in culture is not green fluorescent. (d,e) Frogs were infected with 8.1×10^5 CFU red fluorescent *M. marinum* for 11 weeks followed by superinfection with 2.0×10^6 green fluorescent *M. marinum* or 4.3×10^6 green fluorescent beads. (d) A newly formed granuloma containing only superinfecting green fluorescent *M. marinum*. There is looser aggregation compared with mature lesions in a, b and e. (e) Fluorescent bead trafficking into a preexisting granuloma at 3 d after injection. Arrowheads, superinfecting particles. DAPI-stained tissue nuclei are blue. Scale bars, 50 μm , except for inset in c, 16.7 μm .



data not shown), showing that entry of superinfecting bacteria into granulomas is accomplished by migration of infected host cells.

Mycobacterium-infected monocytes show enhanced trafficking

M. marinum and *M. tuberculosis* stimulate macrophage aggregate formation very early after primary infection^{24,35}. Likewise, in our experiments the superinfecting strain stimulated cellular aggregates within 3 d (Fig. 4d). To determine if the accumulation of mycobacterium-infected cells in granulomas was enhanced compared with that of uninfected phagocytic cells, we compared the rates of accumulation of *M. marinum* versus immunologically inert green fluorescent latex beads. The latter are phagocytosed by but fail to activate mononuclear cells. We injected green fluorescent *M. marinum* or beads into frogs with established red fluorescent *M. marinum* infection and counted the bacteria and beads in pre-established liver granulomas after 3 d. Similar proportions of bacteria and beads reached the liver (Fig. 5a). However, although a few beads were present in the preexisting granulomas (Fig. 4e), the proportion of *M. marinum* trafficking to preexisting granulomas was four- to five-fold greater than that of the beads (Fig. 5a).

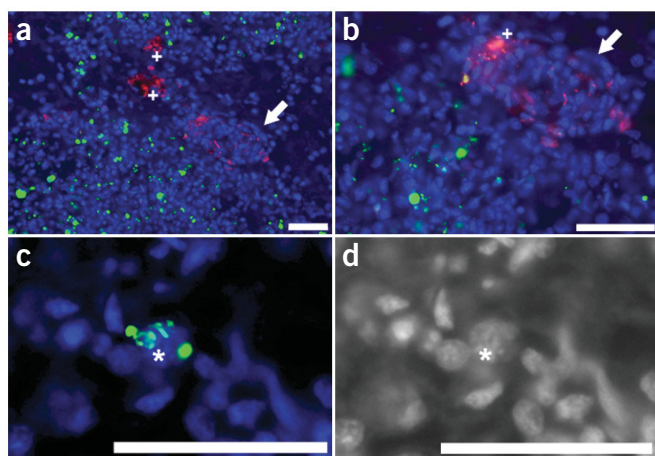


Figure 5 Trafficking of *M. marinum* versus latex beads into pre-established *M. marinum* granulomas. **(a)** Frogs were infected with 8.1×10^5 CFU red fluorescent *M. marinum* for 11 weeks followed by superinfection with 2.0×10^6 green fluorescent *M. marinum* (filled bars; $n = 8$) or 4.3×10^6 green fluorescent beads (open bars; $n = 11$). Then, 3 d later, superinfecting particles were counted per liver (left) and per liver section (right). $P > 0.05$, log mean *M. marinum* versus beads per liver (left). **(b)** Frogs were infected with 2.3×10^6 CFU red fluorescent *M. marinum* for 13.5 weeks and then were superinfected with green fluorescent *M. marinum* plus blue fluorescent beads ($n = 7$) or with beads alone ($n = 4$). For frogs superinfected with *M. marinum* plus beads, both *M. marinum* (black bars) and beads (gray bars) were quantified; for frogs superinfected with beads alone, beads were quantified (open bars). Data were collected as described in **a**. Difference between the log mean beads per liver in the presence or absence of bacteria was not statistically significant (left); no significant difference, *M. marinum* versus beads (coinjection; right); P values, Student's unpaired t -test with Welch correction. Error bars represent s.e.m. Particles quantified: M, *M. marinum*; B, beads; M*, *M. marinum* when coinjected with beads; B*, beads when coinjected with *M. marinum*.

We considered the possibility that the greater number of superinfecting bacteria compared with beads in the pre-established lesions might reflect their preferential replication therein, rather than increased trafficking. To examine this possibility, we compared the rate of entry of beads coinjected with *M. marinum* with that of beads administered alone. To make this comparison, we coinjected blue fluorescent beads with green fluorescent *M. marinum* into frogs with granulomas established by red fluorescent bacteria. We found a greater proportion of beads in the granulomas when they were coinjected with *M. marinum* than when the beads were injected alone (Fig. 5b). Indeed, the entry of coinjected beads was not significantly different from that of *M. marinum* (Fig. 5b). The enhanced entry of beads in the coinjection experiment demonstrated an increased accumulation of mononuclear cells in established granulomas as a result of the *M. marinum* superinfection. Therefore, the greater number of bacteria compared with beads in the preexisting granulomas, when each were injected alone, must also be due to the increased accumulation of infected monocytes rather than to preferential replication of only a few superinfecting bacteria. This increase in cellular traffic is probably due to an enhanced capacity by these infected cells to send or receive chemotactic signals that facilitate their migration. As for the bead and bacteria coinjection experiment, the bacteria may influence bead trafficking in a cell-autonomous manner; that is, beads coinjected with mycobacteria traffic better because of being phagocytosed by the same cell. Alternatively, bead-containing monocytes may demonstrate greater trafficking into granulomas because of a generalized increase in mononuclear cell trafficking induced by the superinfection.

Figure 6 *S. arizonae* is mostly excluded from *M. marinum* granulomas. Frogs were infected with 2.8×10^4 CFU red fluorescent *M. marinum* for 9.5 weeks, then 4.6×10^9 *S. arizonae* were injected and liver tissue was collected after 7 d, and combined fluorescence images of green fluorescent *S. arizonae* and red fluorescent *M. marinum* were obtained. Mean log *S. arizonae* CFU/gram tissue was not statistically different in *M. marinum*-infected (6.49) versus naive (6.86) frogs ($P = 0.33$; Student's unpaired t -test). **(a, b)** Low-magnification **(a)** and high-magnification **(b)** images of a large green *S. arizonae* lesion adjacent to a smaller red *M. marinum* granuloma (arrows). Four sections were examined, each containing 18–20 *M. marinum* granulomas, with no examples of *S. arizonae* trafficking into *M. marinum* granulomas despite the presence of many *S. arizonae* organisms nearby. Similar numbers of green fluorescent *M. marinum* invariably result in mixing. +, tissue autofluorescence. **(c)** Consistent with infection of mice with *Salmonella enterica* serovar Typhimurium³⁶, individual *S. arizonae* seem to be intracellular (*, infected cell nucleus). **(d)** Monochromatic image of DAPI fluorescence from **c**, emphasizing cell nuclei. Scale bars, 50 μ m.

Trafficking is pathogen specific

To further probe the specificity of the enhanced trafficking of mycobacterium-infected cells into granulomas, we examined the localization of *Salmonella enterica* serovar Arizonae (*S. arizonae*), another macrophage pathogen of ectotherms²⁴, with respect to established granulomas in *M. marinum*-infected frogs. Infection of mice with *Salmonella enterica* serovar Typhimurium results in large pockets of infected macrophages in the liver within a few days of infection³⁶. Similarly, in infected frog livers, *S. arizonae*-infected cells were located in many small aggregates scattered throughout the tissue at 3 d (data not shown) and in fewer but much larger aggregates by 7 d (Fig. 6). Coincident with the formation of the large aggregates, we rarely found scattered bacteria at 7 d (Supplementary Table 2 online).

At 3 d after superinfection, a few *S. arizonae* were present in preexisting *M. marinum* granulomas (Table 1, frogs 1 and 2), as was the case with beads (Fig. 5a). However, this trafficking was much less than that of *M. marinum*, as shown by the following competition experiment. We used frogs with established *M. marinum* granulomas, and superinfected these frogs with *M. marinum* and *S. arizonae* simultaneously so as to achieve similar numbers of both organisms in the liver 3 d after superinfection. A much higher proportion of preexisting granulomas

Table 1 Differential trafficking of *M. marinum* and *S. arizonae* into established granulomas

Frog	Superinfecting CFU/gram liver			Superinfecting particles/section		Percent preexisting granulomas containing superinfecting bacteria			
	<i>M. mar.</i>	<i>S. ariz.</i>	<i>M. mar./S. ariz.</i>	<i>M. mar.</i> ^a	<i>S. ariz.</i> ^b	<i>M. mar.</i> only	<i>S. ariz.</i> only	<i>M. mar.</i> and <i>S. ariz.</i>	Normalized ratio ^c
1	NA	1.4×10^6	NA	NA	10^1 – 10^2	NA	2.5	NA	NA
2	NA	9.7×10^6	NA	NA	10^2 – 10^3	NA	17.0	NA	NA
3	8.2×10^5	4.3×10^5	1.9	185	10^1 – 10^2	13	0.3	0.0	23.3
4	3.1×10^6	6.0×10^6	0.5	93	10^2 – 10^3	39	7.0	2.5	8.3
5	1.5×10^6	4.2×10^6	0.4	270	$>10^3$	28	20.3	4.3	3.7
6	1.7×10^7	5.1×10^7	0.3	TNTC	10^2 – 10^3	60	2.8	10.2	16.4
7	5.8×10^6	2.7×10^6	2.1	TNTC	$<10^1$	43	0.4	0.4	164.5

Frogs were infected with red fluorescent *M. marinum* (*M. mar.*) for 11.5 weeks and were superinfected for 3 d with green fluorescent *S. arizonae* (*S. ariz.*; frogs 1 and 2) or green fluorescent *S. arizonae* and dual-labeled (red and green fluorescent) *M. marinum* (frogs 3–7). Two sections, one from each of two different liver lobes, were examined by fluorescence microscopy. NA, not applicable.

^aSuperinfecting *M. marinum* per section were counted except in frogs 6 and 7, reported as TNTC (too numerous to count).

^bNumber of individual *S. arizonae* per section are estimates, as bacteria often clump in individual infected macrophages.

^cNormalized ratio of preexisting *M. marinum* granulomas containing superinfecting *M. marinum* to preexisting *M. marinum* granulomas containing *S. arizonae* was calculated as follows: the total number of granulomas containing *M. marinum* (*M. marinum* only plus *M. marinum* and *S. arizonae*) was divided by the total number of granulomas containing *S. arizonae* (*S. arizonae* only plus *M. marinum* and *S. arizonae*) and this number was normalized to the relative CFU of the two organisms present in the liver.

had superinfecting *M. marinum* than *S. arizonae*, despite similar overall bacterial loads (Table 1, frogs 3–7). This competition experiment further showed that, in contrast to the case with beads (Fig. 5b), trafficking of *S. arizonae* into preexisting granulomas was not increased by simultaneous superinfection with *M. marinum* (Table 1). Conversely, mycobacterium trafficking was also unaffected by *Salmonella* coinfection; the proportion of *M. marinum* trafficking

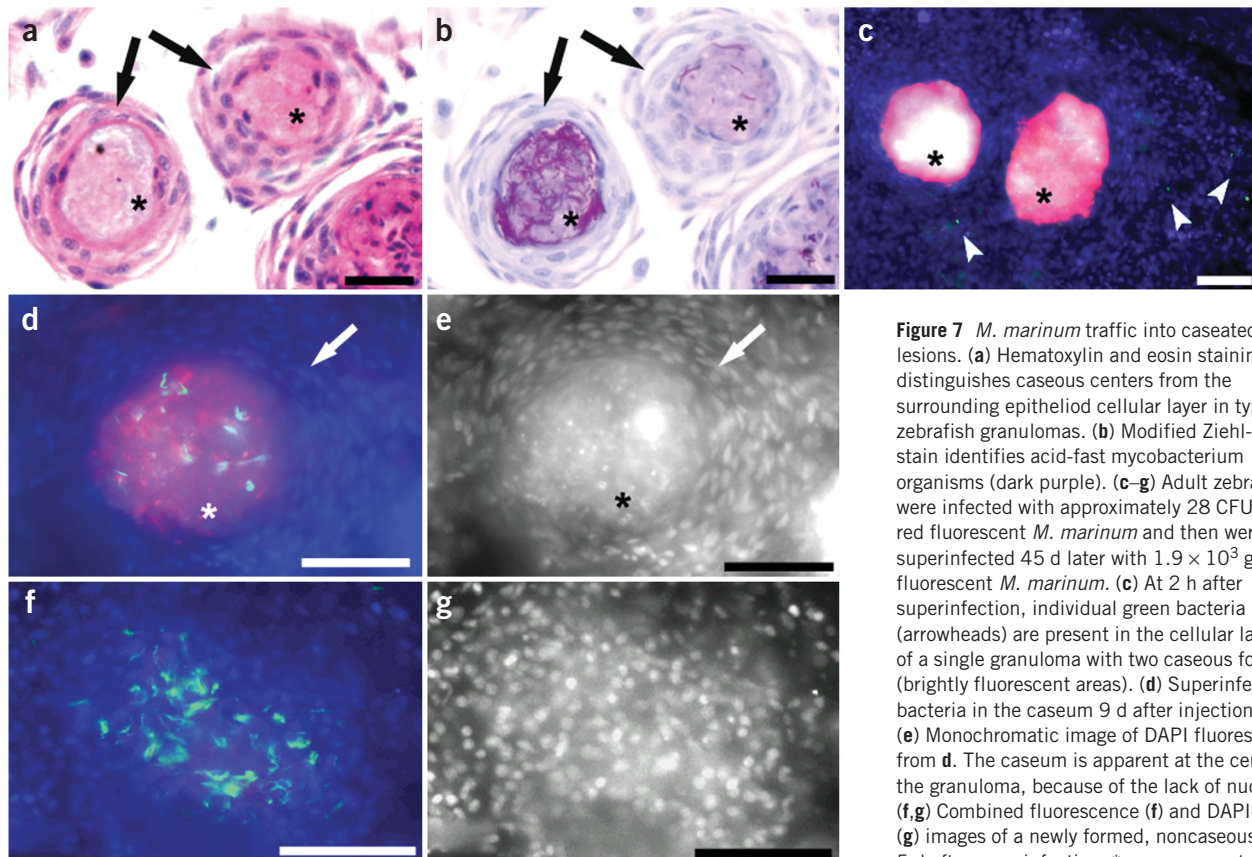


Figure 7 *M. marinum* traffic into caseated fish lesions. (a) Hematoxylin and eosin staining distinguishes caseous centers from the surrounding epithelioid cellular layer in typical zebrafish granulomas. (b) Modified Ziehl-Neelson stain identifies acid-fast mycobacterium organisms (dark purple). (c–g) Adult zebrafish were infected with approximately 28 CFU of red fluorescent *M. marinum* and then were superinfected 45 d later with 1.9×10^3 green fluorescent *M. marinum*. (c) At 2 h after superinfection, individual green bacteria (arrowheads) are present in the cellular layer of a single granuloma with two caseous foci (brightly fluorescent areas). (d) Superinfecting bacteria in the caseum 9 d after injection. (e) Monochromatic image of DAPI fluorescence from d. The caseum is apparent at the center of the granuloma, because of the lack of nuclei. (f, g) Combined fluorescence (f) and DAPI-only (g) images of a newly formed, noncaseous lesion 5 d after superinfection. *, caseous centers; arrows, epithelioid cell layers. Scale bars, 50 μ m.

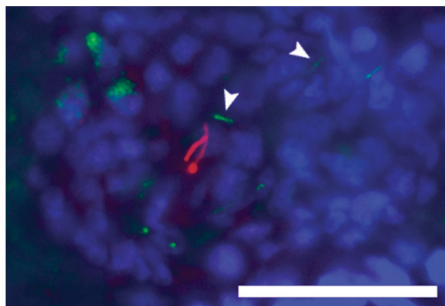


Figure 8 Superinfecting bacteria induce granuloma-specific genes after entry into mature granulomas. A frog was infected with red fluorescent *M. marinum* for 6.5 weeks and then was superinfected with *M. marinum* that express the granuloma-activated *gag7:gfp* promoter fusion. Combined fluorescence image of a liver granuloma 3 d after superinfection shows green fluorescent bacteria in a pre-established granuloma. DAPI-stained host nuclei are blue. Scale bar, 50 μ m.

into established granulomas during the simultaneous superinfection was approximately 25% (data not shown), similar to that seen in *M. marinum*-only superinfections (Fig. 5a). The presence of superinfecting *S. arizonae* in established *M. marinum* granulomas was transient, as by 7 d after superinfection no *S. arizonae* were visible in them (Supplementary Table 2 online). Their disappearance from the *M. marinum* granulomas coincided with their disappearance from the tissues in scattered cells, suggesting that the early trafficking of *S. arizonae*-infected macrophages into pre-established *M. marinum* granulomas is superceded by the formation of the large aggregates. Furthermore, this trafficking was not influenced by the presence of *M. marinum* granulomas in the vicinity. Indeed, even the close juxtaposition of a large *salmonella* granuloma and a smaller mycobacterium granuloma (Fig. 6a) did not result in their comingling (Fig. 6b). In contrast, beads continue to accumulate in established *M. marinum* granulomas even at 8 weeks after superinfection, suggesting that the low level of entry of bead-containing (uninfected) macrophages continued (Supplementary Table 2 online). These results show that comparable superinfection with *M. marinum* and *S. arizonae* of frogs harboring chronic *M. marinum* infection results in distinct localization of the two pathogens with respect to the established granulomas. Therefore, the enhanced trafficking of mycobacterium-infected monocytes into established granulomas is probably due to a pathogen-specific effect and not to their generalized activation.

Superinfecting bacteria penetrate caseum of mature granulomas

One caveat of both the frog infection model used here as well as the mouse model of *M. tuberculosis* infection is that neither system replicates the caseating granulomas found in humans. These lesions represent a more fully developed immune response, and bacteria residing in the caseum are thought to be walled off from host immune cells concentrated in the surrounding granuloma tissue^{10,11,14,37}. To examine directly if superinfecting bacteria traffic to caseous granulomas and whether the caseum itself is penetrated, we examined the trafficking of superinfecting particles in the context of preexisting caseating granulomas in zebrafish. Zebrafish infected with red fluorescent *M. marinum* by intraperitoneal injection developed caseated granulomas in multiple organs by 6 weeks after infection (Fig. 7a,b). Superinfection of these fish with green fluorescent beads showed that the beads reached the caseum by

11 d after injection, the earliest time point examined (data not shown). Similarly, mycobacteria also trafficked into caseous lesions. Superinfecting green fluorescent bacteria reached the cellular layer surrounding the central caseum as early as 2 h after infection (Fig. 7c) and entered the caseum by 5 d (Fig. 7d,e and data not shown). As with the frogs, superinfecting bacteria in the zebrafish also formed their own granulomas by 5 d, although these had not yet developed caseous centers (Fig. 7f,g). These results show that both uninfected and mycobacterium-infected cells rapidly penetrate caseous granulomas, including the caseum itself.

Rapid induction of granuloma-specific genes

Finally, we addressed the issue of how superinfecting mycobacteria that rapidly enter mature granulomas adapt to survive the established host immune response therein. During primary infection, mycobacteria may undergo stepwise adaptations in response to granuloma maturation driven by the host's developing immunity. For instance, *M. marinum* expresses macrophage-activated genes (*mag* genes) after entry into host macrophages and granuloma-activated genes (*gag* genes) only after macrophage aggregation into granulomas^{23,24}. Therefore, we sought to determine if individual superinfecting *M. marinum* expressed *gag* genes immediately after entering mature granulomas. We used frogs with granulomas established by red fluorescent bacteria, and superinfected them with *M. marinum* bearing a *gag7:gfp* fusion. At 3 d after superinfection, we found individual green fluorescent bacteria in preexisting granulomas (Fig. 8). Thus, *gag* expression is rapidly induced when individual bacteria enter established granulomas, exemplifying the generalized rapid adaptation of superinfecting bacteria to the granuloma environment.

DISCUSSION

We have probed the mechanisms of mycobacterial reinfection in the context of tuberculous granulomas in frogs and zebrafish. The *M. marinum* frog model is particularly suitable for the study of trafficking into granulomas, as infection results in chronic granulomas that remain well organized over long time periods. This pathology is in contrast to the mouse model of tuberculosis, in which even low infectious doses of *M. tuberculosis* result in progressive disease characterized by highly inflammatory granuloma-like aggregates that often coalesce over the period of a few weeks³⁸. In addition, the use of zebrafish permits observation of caseating granulomas, another feature of human disease lacking in the mouse model. We found that rather than being excluded from established granulomas, superinfecting mycobacteria were rapidly transported to these foci by host mononuclear cells. It is possible that the rapid transport that we noted is infrequent in those natural infections with few preexisting granulomas. However, our findings demonstrate previously unknown aspects of the mycobacterium-host interaction.

The enhanced migration to granulomas of mycobacterium-infected phagocytes compared with that of uninfected phagocytes is notable, particularly given the tendency of mycobacterium-infected cells to aggregate into new lesions in the same time frame. These data suggest that established granulomas compete effectively for mycobacterium-infected monocytes that are programmed to form their own aggregates in a naive host. Although uninfected cells show a basal level of entry into foci of infection, mycobacterium infection enhances recognition of these foci, suggesting a previously unrecognized cell-cell crosstalk between the complex adaptive immune milieu of the granuloma and individual infected innate immune cells. This communication is probably mediated by

specific expression of cytokines and/or cytokine receptors as well as adhesion molecules in both the granuloma and the individual infected monocytes and may be directly induced by bacterial components. Although our results did not distinguish between enhanced entry and enhanced retention of mycobacterium-infected monocytes versus uninfected monocytes, both models indicate a previously unrecognized specific affinity between individual mycobacterium-infected cells and tuberculous granulomas.

Similarly, the exclusion of salmonella-infected cells from mycobacterium granulomas further demonstrates that mononuclear cells infected by different pathogens pursue distinct trafficking patterns. The disappearance of *S. arizonae* from *M. marinum* granulomas between 3 and 7 d could be due to their selective killing within the *M. marinum* granulomas or to the efflux of the *S. arizonae*-infected cells to follow their own trafficking program. Either possibility has relevant implications: complete killing of superinfecting salmonella (but not of superinfecting mycobacterium) within an immunological structure developed to counter mycobacterium infection is particularly notable, given that superinfecting salmonella continue to grow in their own granulomas. Efflux would suggest differential adhesion properties of salmonella-infected versus bead-containing (uninfected) macrophages. Whatever the fate of the salmonella that had entered by 3d, their complete absence from the granulomas at 7 d shows that new bacteria had stopped entering in by the 7-day time point. Our findings show that innate immune cells such as macrophages and dendritic cells may also have distinct localization patterns because of antigen- or pathogen-mediated differences. Such differential homing has thus far been ascribed only to cells of the adaptive immune system³⁹. Markers to distinguish macrophages and dendritic cells are not yet available in the zebrafish, but such immunological tools are being developed rapidly in this new model host.

If this rapid delivery of the incoming pathogen to areas of enhanced adaptive immunity represents a host defense mechanism, it is ineffective at eliminating the superinfecting organisms. Our results directly contradict those of previous models attributing tuberculosis resulting from reinfection to the ability of reinfecting mycobacteria to physically evade the foci of established host immunity^{16,17}. Because adaptive immunity is necessary for the prevention of more-lethal disseminated tuberculosis², the tenet of vaccine strategies so far has been that improving the immunogenicity or persistence of vaccine strains can enhance adaptive immunity to achieve clinically important protection, at least against reinfecting bacteria⁷⁻⁹. However, we have shown that as with the original infecting strain, the granuloma fails to eradicate superinfecting bacteria. Thus, there seems to be no escalation in the potency of adaptive immunity as the primary infection becomes chronic, and even 'naive' mycobacteria are not eliminated in this concentrated focus of adaptive immunity.

The granuloma has long been an ill-understood immunological and pathological entity with regard to its accessibility to incoming cellular traffic⁴⁰. In particular, the function of the caseum in human tuberculosis remains enigmatic. Yet despite this lack of clarity, the caseum features prominently in many models of mycobacterial persistence^{10,11,14,41}. Itself a paradox, the caseum is thought to be both an antimycobacterial compartment, wherein bacterial growth is restricted, and a specialized niche for the long-term persistence of latent organisms^{10,11,14}. Models of tuberculosis suggest that the caseum and the bacteria therein constitute a relatively insulated area in which bacteria interact only with the immediately surrounding macrophages¹¹. However, the extent to which caseous foci are isolated from the surrounding tissue has not been

addressed experimentally. We found that bacteria were quickly transported across multiple cellular layers of the granuloma to enter the caseum. This finding suggests that caseating granulomas, in particular the caseum itself, produce signals to attract infected and uninfected monocytes. It further shows that the caseum itself is not physically walled off from the surrounding tissue, given that mononuclear cells continue to enter. These findings show that the caseous foci of mycobacterial lesions are more dynamic than has been previously appreciated.

Our data also speak indirectly to mechanisms of mycobacterium persistence. Mycobacterial persistence has been attributed to the ability of the pathogen to gradually enter a nonreplicative and metabolically quiescent state. This state is thought to be achieved only by a gradual adaptation of the bacteria to evolving host responses^{1,41}. Certainly changes in gene transcription occur when bacteria are present in mature granulomas *in vivo*^{23,26,42}, which may be important for their adaptation. However, our finding that superinfecting mycobacteria rapidly enter preexisting foci of infection yet persist long term therein contradicts the prevailing assumption that persistence develops gradually only in a population of bacteria present from the initial founding of the granuloma. Entry is accompanied by the rapid induction of at least some genes that correlate with residence in granulomas *in vivo*. Thus, it seems that mycobacterium adaptation mechanisms initiate rapidly so as to ensure survival in the context of the mature granuloma environment.

Diverse mechanisms may dampen host immunity during mycobacterial infections as is being discovered for other chronic infections. Regulatory T cells in chronic leishmaniasis prevent clearing of the existing infection while maintaining immunity to reinfection⁴³. In contrast, chronicity of mouse lymphocytic choriomeningitis infection correlates with loss of CD8 T cell effector function⁴⁴. Our results contribute to a growing understanding that adaptive immunity to persistent pathogens is fundamentally different from immunity to pathogens that are efficiently cleared. Efforts must be directed at a deeper understanding of the immunological crosstalk that ultimately leads to incomplete protection against both primary and reinfection tuberculosis. Our findings, which contradict current models of mycobacterial reinfection and persistence, suggest that the elimination and prevention of tuberculosis will be more complex than previously appreciated. Consequently, a thorough reevaluation of strategies for the development of an improved tuberculosis vaccine is warranted.

METHODS

Bacteria. *M. marinum* strains expressed green (GFP), red (dsRed2; Clontech) or cyan fluorescent protein from the constitutive *msp11* and *msp12* promoters or expressed GFP from host-inducible (*mag49* and *gag7*) promoters^{23,26}. *S. arizonae* (a gift from S. Miller, University of Washington, Seattle, Washington) expresses a constitutive GFP fusion.

Animals and infections. Adult male *Rana pipiens* (J.M. Hazen) were infected by intraperitoneal injection of log-phase *M. marinum* culture¹⁹, stationary-phase *S. arizonae* culture (concentrated tenfold) or 1- μ m Fluoresbrite YG or BB microspheres (Polysciences) suspended in PBS. Inoculation doses for individual experiments are in the figure legends. For the simultaneous superinfection of *S. arizonae* and *M. marinum* in Table 1, frogs were superinfected with 4.5×10^9 colony-forming units (CFU) *S. arizonae* plus either 3.6×10^6 CFU *M. marinum* or 1.2×10^7 CFU *M. marinum*. Frogs for which the liver burden of the two superinfecting strains was within twofold of each other were selected for further analysis. In all experiments, tissue bacterial counts were determined by plating of serial dilutions of tissue homogenates as described¹⁹. For tissue bead counts, 1 μ l of tissue homogenate was spotted onto a hemocytometer slide and the total

number of beads in this volume was determined by fluorescence microscopy. Wild-type *Danio rerio* (Zebrafish International Resource Center) were anaesthetized in 0.01% tricaine for about 1 min, then were infected by intraperitoneal injection, using a 30-gauge needle, with 50 μ l bacterial stock or beads as prepared for frogs. All experiments were done in compliance with institutional guidelines of the University of Washington (Seattle, Washington).

Tissue sections and microscopy. Frozen sections of both frog tissues and whole zebrafish, 10 μ m in thickness, were stained with SlowFade Antifade reagent plus DAPI (4,6-diamidino-2-phenylindole; Molecular Probes) before being imaged with a Nikon E600 microscope and analyzed with a Metamorph software package (Universal Imaging). For histological analyses, frog tissues or whole zebrafish were embedded in paraffin. Sections 5 μ m in thickness were stained with hematoxylin and eosin or with Ziehl-Neelson acid-fast stain by Histo-Tec Laboratory. Statistical analysis was done with GraphPad InStat version 3.05 for Windows.

Note: Supplementary information is available on the Nature Immunology website.

ACKNOWLEDGMENTS

We thank K. Klein for technical assistance; K. Klein and P. Carroll for constructing plasmids; K. Urdahl, S. Miller, D. Sherman, M. Kaja, C. Wilson, M. Bevan and N. Salama for discussions; A. Farr and J. Dooley for tissue cryosectioning advice and equipment; D. Lauman for advice on statistics; and K. Urdahl, M. Kaja, T. Pozos and D. Tobin for comments on the manuscript. Supported by National Institutes of Health (R01 AI 36396) and an Ellison Medical Foundation New Scholar in Global Infectious Diseases award (L.R.).

COMPETING INTERESTS STATEMENT

The authors declare that they have no competing financial interests.

Received 5 February; accepted 17 May 2004

Published online at <http://www.nature.com/natureimmunology/>

- Parrish, N.M., Dick, J.D. & Bishai, W.R. Mechanisms of latency in *Mycobacterium tuberculosis*. *Trends Microbiol.* **6**, 107–112 (1998).
- Flynn, J.L. & Chan, J. Immunology of tuberculosis. *Annu. Rev. Immunol.* **19**, 93–129 (2001).
- Cosma, C.L., Sherman, D.R. & Ramakrishnan, L. The secret lives of the pathogenic mycobacteria. *Annu. Rev. Microbiol.* **57**, 641–676 (2003).
- Stead, W.W. Pathogenesis of a first episode of chronic pulmonary tuberculosis in man: recrudescence of residuals of the primary infection or exogenous reinfection? *Am. Rev. Respir. Dis.* **95**, 729–745 (1967).
- Caminero, J.A. *et al.* Exogenous reinfection with tuberculosis on a European island with a moderate incidence of disease. *Am. J. Respir. Crit. Care Med.* **163**, 717–720 (2001).
- van Rie, A. *et al.* Exogenous reinfection as a cause of recurrent tuberculosis after curative treatment. *N. Engl. J. Med.* **341**, 1174–1179 (1999).
- Kaufmann, S.H. How can immunology contribute to the control of tuberculosis? *Nat. Rev. Immunol.* **1**, 20–30 (2001).
- Sambandamurthy, V.K. *et al.* A pantothenate auxotroph of *Mycobacterium tuberculosis* is highly attenuated and protects mice against tuberculosis. *Nat. Med.* **8**, 1171–1174 (2002).
- Pym, A.S. *et al.* Recombinant BCG exporting ESAT-6 confers enhanced protection against tuberculosis. *Nat. Med.* **9**, 533–539 (2003).
- Grosset, J. *Mycobacterium tuberculosis* in the extracellular compartment: an underestimated adversary. *Antimicrob. Agents Chemother.* **47**, 833–836 (2003).
- Dannenbergs, A.M., Jr. Immunopathogenesis of pulmonary tuberculosis. *Hosp. Pract.* **28**, 51–58 (1993).
- Lawn, S.D., Butera, S.T. & Shinnick, T.M. Tuberculosis unleashed: the impact of human immunodeficiency virus infection on the host granulomatous response to *Mycobacterium tuberculosis*. *Microbes Infect.* **4**, 635–646 (2002).
- Frieden, T.R., Sterling, T.R., Munsiff, S.S., Watt, C.J. & Dye, C. Tuberculosis. *Lancet* **362**, 887–899 (2003).
- Dannenbergs, A.M., Jr. Macrophage turnover, division and activation within developing, peak and “healed” tuberculous lesions produced in rabbits by BCG. *Tuberculosis (Edinb.)* **83**, 251–260 (2003).
- Hernandez-Pando, R. *et al.* Persistence of DNA from *Mycobacterium tuberculosis* in superficially normal lung tissue during latent infection. *Lancet* **356**, 2133–2138 (2000).
- Balasubramanian, V., Wiegand, E.H., Taylor, B.T. & Smith, D.W. Pathogenesis of tuberculosis: pathway to apical localization. *Tuber. Lung Dis.* **75**, 168–178 (1994).
- McMurray, D.N. Hematogenous reseeding of the lung in low-dose, aerosol-infected guinea pigs: unique features of the host-pathogen interface in secondary tubercles. *Tuberculosis (Edinb.)* **83**, 131–134 (2003).
- Opie, E.L. & Aronson, J.D. Tubercle bacilli in latent tuberculous lesions and in lung tissue without tuberculous lesions. *Arch. Pathol. Lab. Med.* **4**, 1–21 (1927).
- Ramakrishnan, L., Valdivia, R.H., McKerrow, J.H. & Falkow, S. *Mycobacterium marinum* causes both long-term subclinical infection and acute disease in the leopard frog (*Rana pipiens*). *Infect. Immun.* **65**, 767–773 (1997).
- Ramakrishnan, L. Using *Mycobacterium marinum* and its hosts to study tuberculosis. *Curr. Sci.* **86**, 82–92 (2004).
- Talaat, A.M., Reimschuessel, R., Wasserman, S.S. & Trucksis, M. Goldfish, *Carassius auratus*, a novel animal model for the study of *Mycobacterium marinum* pathogenesis. *Infect. Immun.* **66**, 2938–2942 (1998).
- Traver, D. *et al.* The zebrafish as a model organism to study development of the immune system. *Adv. Immunol.* **81**, 253–330 (2003).
- Chan, K. *et al.* Complex pattern of *Mycobacterium marinum* gene expression during long-term granulomatous infection. *Proc. Natl. Acad. Sci. USA* **99**, 3920–3925 (2002).
- Davis, J.M. *et al.* Real-time visualization of *Mycobacterium*-macrophage interactions leading to initiation of granuloma formation in zebrafish embryos. *Immunity* **17**, 693–702 (2002).
- Bouley, D.M., Ghori, N., Mercer, K.L., Falkow, S. & Ramakrishnan, L. Dynamic nature of host-pathogen interactions in *Mycobacterium marinum* granulomas. *Infect. Immun.* **69**, 7820–7831 (2001).
- Ramakrishnan, L., Federspiel, N.A. & Falkow, S. Granuloma-specific expression of *Mycobacterium* virulence proteins from the glycine-rich PE-PGRS family. *Science* **288**, 1436–1439 (2000).
- Gao, L.Y. *et al.* Requirement for *kasB* in *Mycobacterium mycolic acid* biosynthesis, cell wall impermeability and intracellular survival: implications for therapy. *Mol. Microbiol.* **49**, 1547–1563 (2003).
- Stamm, L.M. *et al.* *Mycobacterium marinum* escapes from phagosomes and is propelled by actin-based motility. *J. Exp. Med.* **198**, 1361–1368 (2003).
- Ohl, M.E. & Miller, S.I. Salmonella: A model for bacterial pathogenesis. *Annu. Rev. Med.* **52**, 259–274 (2001).
- Repique, C.J., Li, A., Collins, F.M. & Morris, S.L. DNA immunization in a mouse model of latent tuberculosis: effect of DNA vaccination on reactivation of disease and on reinfection with a secondary challenge. *Infect. Immun.* **70**, 3318–3323 (2002).
- Ziegler, J.E., Edwards, M.L. & Smith, D.W. Exogenous reinfection in experimental airborne tuberculosis. *Tubercle* **66**, 121–128 (1985).
- Tailleux, L. *et al.* DC-SIGN is the major *Mycobacterium tuberculosis* receptor on human dendritic cells. *J. Exp. Med.* **197**, 121–127 (2003).
- Teitelbaum, R. *et al.* The M cell as a portal of entry to the lung for the bacterial pathogen *Mycobacterium tuberculosis*. *Immunity* **10**, 641–650 (1999).
- Geijtenbeek, T.B. *et al.* Mycobacteria target DC-SIGN to suppress dendritic cell function. *J. Exp. Med.* **197**, 7–17 (2003).
- Roach, D.R., Briscoe, H., Baumgart, K., Rathjen, D.A. & Britton, W.J. Tumor necrosis factor (TNF) and a TNF-mimetic peptide modulate the granulomatous response to *Mycobacterium bovis* BCG infection *in vivo*. *Infect. Immun.* **67**, 5473–5476 (1999).
- Richter-Dahlfors, A., Buchan, A.M. & Finlay, B.B. Murine salmonellosis studied by confocal microscopy: *Salmonella typhimurium* resides intracellularly inside macrophages and exerts a cytotoxic effect on phagocytes *in vivo*. *J. Exp. Med.* **186**, 569–580 (1997).
- Janeway, C.A., Travers, P., Walport, M. & Shlomchik, M. *Immunobiology* (Garland Publishing, New York, 2001).
- Rhoades, E.R., Frank, A.A. & Orme, I.M. Progression of chronic pulmonary tuberculosis in mice aerogenically infected with virulent *Mycobacterium tuberculosis*. *Tuber. Lung Dis.* **78**, 57–66 (1997).
- von Andrian, U.H. & Mempel, T.R. Homing and cellular traffic in lymph nodes. *Nat. Rev. Immunol.* **3**, 867–878 (2003).
- Adams, D.O. The granulomatous inflammatory response. A review. *Am. J. Pathol.* **84**, 164–191 (1976).
- Wayne, L.G. & Sohaskey, C.D. Nonreplicating persistence of *Mycobacterium tuberculosis*. *Annu. Rev. Microbiol.* **55**, 139–163 (2001).
- Fenhalls, G. *et al.* *In situ* detection of *Mycobacterium tuberculosis* transcripts in human lung granulomas reveals differential gene expression in necrotic lesions. *Infect. Immun.* **70**, 6330–6338 (2002).
- Belkaid, Y., Piccirillo, C.A., Mendez, S., Shevach, E.M. & Sacks, D.L. CD4⁺CD25⁺ regulatory T cells control *Leishmania major* persistence and immunity. *Nature* **420**, 502–507 (2002).
- Wherry, E.J., Blattman, J.N., Murali-Krishna, K., van der Most, R. & Ahmed, R. Viral persistence alters CD8 T-cell immunodominance and tissue distribution and results in distinct stages of functional impairment. *J. Virol.* **77**, 4911–4927 (2003).

